Available online at www.sciencedirect.com
ScienceDirect
Journal of Computational Physics 226 (2007) 1102–1121
JOURNAL OF COMPUTATIONAL PHYSICS
www.elsevier.com/locate/jcp

A method of constructing adaptive hexahedral moving grids

Boris N. Azarenok *

Dorodnicyn Computing Center of the Russian Academy of Sciences, Vavilov str. 40, GSP-1, Moscow 119333, Russia

Received 18 November 2006; received in revised form 7 May 2007; accepted 9 May 2007
Available online 24 May 2007

Abstract

A variational method of constructing an adaptive moving grid composed of hexahedral cells is considered. The method is based on minimizing a functional defined on the Riemannian manifold in space of variables including the physical space coordinates and components of a vector-valued monitor function. The mesh is generated in the manifold and then it is projected down to the physical region to provide the adaptive grid. The integrand of the functional is the non-dimensional ratio of the invariants of the metric. The functional depends on metric elements of two metrics. The curvilinear mesh, generated in the manifold, induces the monitor metric. Another control metric, defined in a special way, is responsible for additional cell shape control. The issues of non-degeneracy conditions for a hexahedral mesh are considered. Examples of adaptive grids are presented.

Keywords: Moving adaptive mesh; Minimization of functional; Monitor metric; Control metric; Infinite barrier

1. Introduction

Adaptive grids, being condensed in subdomains of high gradients of the monitor function, allow significant improvement in the accuracy of physical modeling. One promising development is the use of moving grids, since they can preserve a simple mesh structure which, in turn, simplifies the numerical procedure of solving a physical problem. When employing a variational approach, the grid lines in 2-D and grid surfaces in 3-D are smooth. Those methods allow the execution of additional control for the cell shape by applying specific functionals. Description of some variational adaptive mesh methods and applications can be found, for instance, in the monographs [1–6], surveys [7–11], papers [12–22], and others. Generally, in the adaptive mesh approach, the equidistribution principle is employed for the error estimates of the solution or for geometrical parameters of the monitor surface. In [13], the source terms in the Poisson equations are expressed in terms of weight functions that measure the flow activity along grid lines. In [14], a special Riemannian metric is introduced via the monitor function and further, in [21], this idea was implemented when constructing the harmonic mapping of the parametric square onto the manifold. In [15], it was proposed that the functional of smoothness should be

* Tel.: +7 495 1356498; fax: +7 495 1356159.
E-mail address: azarenok@ccas.ru

0021-9991/$ - see front matter
doi:10.1016/j.jcp.2007.05.010

defined on the monitor surface. This idea is employed in the methods considered in [17–20,22,23]. In [23], the dimensional functional of smoothness, proposed in [15], was applied for constructing 3-D adaptive hexahedral grids. In [6], the Euler–Lagrange equations for that functional were employed with the same purpose. In [16], the 2-D mesh is adapted in the parametric domain. The level-set-based deformation method for generating adaptive moving grids was developed in [24].

When adapting the mesh in realistic, complicated domains, grid non-degeneracy is one more requirement of particular importance. A special class of the barrier variational methods, introduced in grid generation in [25], automatically guarantee mesh non-degeneracy in the course of computation. It was suggested that the barrier method could be applied to adaptive mesh construction in [3,17,23]. In [19], a special way of freezing the metric was considered so as to preserve the barrier property of the discrete functional in problems with a discontinuous monitor function. A second parametrization was proposed in [26] with the objective of employing a control for the cell shape. This idea was applied to adaptive meshes in [27,31].

In this paper, we present the adaptive moving mesh method for grids composed of hexahedral (hex) cells. The method is based on minimizing a functional defined on the Riemannian manifold in space of variables including the physical space coordinates and components of a vector-valued monitor function. The mesh is generated in the manifold and then projected down to the physical region to provide the adaptive grid. The integrand of the functional is the non-dimensional ratio of the invariants of metric. The functional depends on metric elements of two metrics. The curvilinear mesh, generated in the manifold, induces the monitor metric. Another control metric, defined in a special spirit, is responsible for additional cell shape control. For each hex cell, the functional is discretized on 10 tetrahedra forming two dodecahedra with the same vertices that span the hex cell. The discrete functional possesses an infinite barrier on the boundary of the set of non-folded dodecahedral cells that ensures the construction of a non-folded grid composed of such cells. In its practical implementation, the corresponding hexahedral mesh is also non-folded.

The outline of the paper is as follows: in Section 2, the adaptive grid problem formulation is given and functional is constructed in the general n-dimensional case. Section 3 presents the 3-D functional. Sections 4 and 5 discuss non-degeneracy conditions for a mesh and hex cell, respectively. Section 6 specifies the way of discretizing the functional and discusses the barrier property. The minimizing procedure for the discrete functional is described in Section 7 and computational formulae are given in Section 8. The method of boundary nodes redistribution is presented in Section 9. Two examples of grid construction are reported in Section 10. In Section 11, the case of a discontinuous monitor function is analyzed.

2. Problem formulation and variational functional

Let a Riemannian manifold $\mathcal{M}$ be given in the space $\mathbb{R}^{n+m}$ of variables $\mathbf{x} = (x^1,\dots,x^n,f^1,\dots,f^m) = (x^1,\dots,x^{n+m})$. Here n is the dimension of Euclidian space $\mathbb{R}^n$ of the variables $\tilde{\mathbf{x}} = (x^1,\dots,x^n)$, m is the number of components of the vector-valued monitor function $\mathbf{f} = (f^1,\dots,f^m)$ being used for grid adaptation. Every component of $\mathbf{f}$ depends on $\tilde{\mathbf{x}}$, i.e., $f^p = f^p(x^1,\dots,x^n)$, $p = 1,\dots,m$. For instance in a flow problem, as f^p one may employ the density, pressure, velocity components, etc.

Consider a homeomorphic smooth, $\mathbb{C}^1$, mapping $\mathbf{x}(\mathbf{X}) : \mathbb{R}^n \to \mathbb{R}^{n+m}$ of the canonical domain $\mathcal{C}$ in space of the variables $\mathbf{X} = (X^1,\dots,X^n)$ onto the manifold $\mathcal{M}$ with the Jacobian matrix $a^i_j = \partial x^i/\partial X^j$, $i = 1,\dots,n+m$, $j = 1,\dots,n$. Consider also an analogous auxiliary mapping $\mathbf{x}(\boldsymbol{\xi}) : \mathbb{R}^n \to \mathbb{R}^{n+m}$ of the parametric domain $\mathcal{P}$ in space of the variables $\boldsymbol{\xi} = (\xi^1,\dots,\xi^n)$ (as a rule it is the unit cube $0 \leqslant \xi^1,\dots,\xi^n \leqslant 1$) onto the manifold $\mathcal{M}$ with the Jacobian matrix $b^i_j = \partial x^i/\partial \xi^j$, $i = 1,\dots,n+m$, $j = 1,\dots,n$, and auxiliary mapping $\mathbf{X}(\boldsymbol{\xi}) : \mathbb{R}^n \to \mathbb{R}^n$ of the domain $\mathcal{P}$ onto $\mathcal{C}$ with the Jacobian matrix $c^i_j = \partial X^i/\partial \xi^j$, $i,j = 1,\dots,n$. The domains $\mathcal{P},\mathcal{C}$ and manifold $\mathcal{M}$ are assumed to be simply connected and bounded. In order to derive the functional, the transformation $\mathbf{x}(\mathbf{X})$ will be expressed via composition of two auxiliary mappings: inverse $\boldsymbol{\xi}(\mathbf{X})$ and direct $\mathbf{x}(\boldsymbol{\xi})$. If in the domain $\mathcal{C}$, we have a non-folded curvilinear mesh (for mesh non-degeneracy see Section 4), given by the node coordinates $\mathbf{X}_l$ (l is the node number), then its image in $\mathcal{M}$ is also a non-folded mesh. The projection of the latter down to the physical domain Ω in the space $\mathbb{R}^n$ of variables $\tilde{\mathbf{x}}$ is an adaptive grid. The mapping of the nodal points $\mathbf{x}(\mathbf{X}_l)$ is called a discrete mapping.

In Fig. 1, we present an example of the case $n = 2$, $m = 1$, i.e., with the scalar monitor function f. The domain $\mathcal{P}$, the unit parametric square in the plane ξ^1,ξ^2, is mapped onto the domain $\mathcal{C}$ in the plane X^1, X^2.

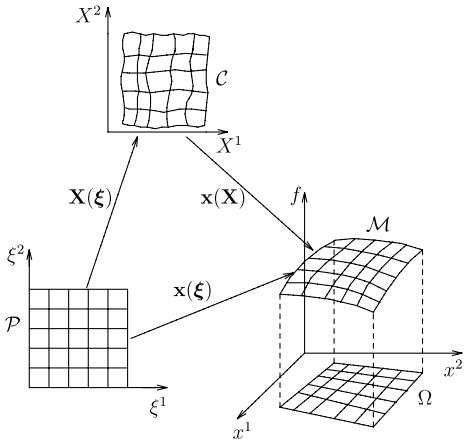

Fig. 1. Case $n = 2$, $m = 1$. Manifold $\mathcal{M}$ is a surface in $\mathbb{R}^3$ space x^1, x^2, f. $\mathcal{P}, \mathcal{C}, \Omega$ are the parametric, canonical, and physical domains, respectively.

$\mathcal{P}$ and $\mathcal{C}$ are mapped onto the manifold $\mathcal{M}$, being a surface in $\mathbb{R}^3$ space of the variables x^1, x^2, f. The curvilinear mesh, given in $\mathcal{C}$, is transformed to the mesh in $\mathcal{M}$ by the mapping $\mathbf{x}(\mathbf{X})$ and the projection of the latter down to the plane x^1, x^2 is the adaptive mesh in the 2-D physical domain Ω. The case $n = 1$, $m = 2$ is shown in Fig. 2. The monitor function has two components $\mathbf{f} = (f^1, f^2)$. The unit segment $\mathcal{P}$ in the ξ-axis is mapped onto the segment $\mathcal{C}$ in the X-axis, and each of them is mapped onto the manifold $\mathcal{M}$, being a curve in $\mathbb{R}^3$ space of the variables x, f^1, f^2. The projection of the mesh, constructed on the curve $\mathcal{M}$ by the mapping $\mathbf{x}(X)$, down to the x-axis is the adaptive mesh in the 1-D domain Ω.

Adaptive mesh generation is employed by means of the homeomorphic smooth, $\mathbb{C}^1$, mapping $\mathbf{x}(\mathbf{X}) : \mathbb{R}^n \to \mathbb{R}^{n+m}$ of the domain $\mathcal{C}$ onto the manifold $\mathcal{M}$, provided that the boundary correspondence is given. The functions $\mathbf{x}(\mathbf{X})$, executing this mapping, are sought by minimizing a functional. The functional is the integral of a function depending on the invariants of the metric $h = a^\top a$ ($a^\top$ is the transposed Jacobian matrix) induced by this mapping. The invariants of h can be expressed in terms of the invariants of the tensor $G^{-1}g$ where the metrics $g = b^\top b$ and $G = c^\top c$ are induced by the mappings $\mathbf{x}(\boldsymbol{\xi})$ and $\mathbf{X}(\boldsymbol{\xi})$, respectively (see [28]). In particularly, we employ the invariants $I_1 = \mathrm{tr}(G^{-1}g)$ and $I_n = \det(G^{-1}g)$.

Consider the ratio of the invariant I_1 to I_n raised to an appropriate power and normalised so as to obtain a non-dimensional function

$$E = \frac{1}{n^{n/2}} \frac{I_1^{n/2}}{I_n^{1/2}} = \frac{1}{n^{n/2}} \frac{(\mathrm{tr}(G^{-1}g))^{n/2} \sqrt{\det G}}{\sqrt{\det g}} \tag{1}$$

and write the following functional for E being the integral over the n-dimensional unit cube

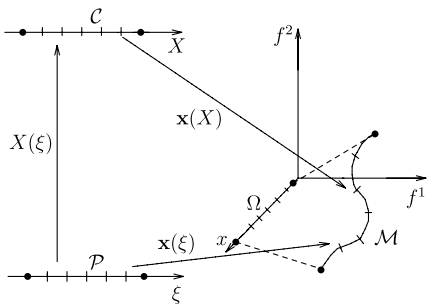

Fig. 2. Case $n = 1$, $m = 2$. Manifold $\mathcal{M}$ is a curve in $\mathbb{R}^3$ space x, f^1, f^2.

$$\mathcal{D}(\mathbf{x}(\boldsymbol{\xi})) = \int_0^1 E \, \mathrm{d}\xi^1 \cdots \mathrm{d}\xi^n = \frac{1}{n^{n/2}} \int_0^1 \frac{(\mathrm{tr}(G^{-1}g))^{n/2}\sqrt{\det G}}{\sqrt{\det g}} \, \mathrm{d}\xi^1 \cdots \mathrm{d}\xi^n. \tag{2}$$

$\mathcal{D}$ is the invariant to an orthogonal transformation and scaling of the coordinate systems $\mathbf{x}$ and $\mathbf{X}$. For non-adaptive grid construction, when all components $f^p = \text{const.}$ and the manifold $\mathcal{M}$ is a physical domain Ω, the functional in the form (2) was suggested in [29].

In practical implementation, generally, it is convenient to use one more variational formulation of the adaptive grid generation problem [28]. It is sought a homeomorphic smooth, $\mathbb{C}^1$, mapping $\mathbf{x}(\boldsymbol{\xi}) : \mathbb{R}^n \to \mathbb{R}^{n+m}$ of the parametric domain $\mathcal{P}$ onto the manifold $\mathcal{M}$ provided that the boundary correspondence is given. The functions $\mathbf{x}(\boldsymbol{\xi})$, executing the mapping, are sought which minimize the functional (2). $G_{ij}(\boldsymbol{\xi})$ are the elements of a symmetric positive definite matrix given at every point in $\mathcal{P}$. In the 2-D case, analogous formulations were employed, for instance, in [26,27,30–32].

3. Three-dimensional functional

In the case $n = 3$, the functional (2) reads

$$\mathcal{D} = \frac{1}{3^{3/2}} \int_0^1 \int_0^1 \int_0^1 \frac{(\mathrm{tr}(G^{-1}g))^{3/2}\sqrt{\det G}}{\sqrt{\det g}} \, \mathrm{d}\xi^1 \, \mathrm{d}\xi^2 \, \mathrm{d}\xi^3, \tag{3}$$

where

$$\mathrm{tr}(G^{-1}g) = G^{ij}g_{ji} = G^{11}g_{11} + G^{22}g_{22} + G^{33}g_{33} + 2G^{12}g_{12} + 2G^{13}g_{13} + 2G^{23}g_{23},$$

G^{ij} are the elements of the inverse matrix G^{-1} (contravariant tensor) and the summation convention is applied over repeated indices. On the manifold $\mathcal{M}$ in $\mathbb{R}^{3+m}$ at a point with coordinates $\mathbf{r} = (x^1, x^2, x^3, f^1, \ldots, f^m)$, the elements of the metric tensor g are

$$g_{ij} = (\mathbf{r}_{\xi^i} \cdot \mathbf{r}_{\xi^j}), \quad i, j = 1, 2, 3, \tag{4}$$

where $\mathbf{r}_{\xi^i} = (x^1_{\xi^i}, x^2_{\xi^i}, x^3_{\xi^i}, f^1_{\xi^i}, \ldots, f^m_{\xi^i})$. $\mathcal{M}$ is a monitor manifold, therefore, g may be called a monitor metric. Since every component $f^p = f^p(x^1, x^2, x^3)$ and, therefore,

$$f^p_{\xi^i} = f^p_{x^j} x^j_{\xi^i}, \quad i, j = 1, 2, 3, \ p = 1, \ldots, m, \tag{5}$$

the metric elements are

$$g_{ij} = \alpha_{kl} \frac{\partial x^k}{\partial \xi^i} \frac{\partial x^l}{\partial \xi^j}, \tag{6}$$

where

$$\alpha_{kl} = \delta_{kl} + \sum_{p=1}^{m} \frac{\partial f^p}{\partial x^k} \frac{\partial f^p}{\partial x^l}, \quad k, l = 1, 2, 3, \tag{7}$$

and δ_{kl} is the Kronecker delta. The elements of the metric tensor G at a point in space X^1, X^2, X^3 are defined analogously to (4).

Let us derive the expression for the determinant of the metric tensor g. Substituting the coefficients (6) and (7) in $\det g$, after rather a cumbersome algebraic derivation (omitted for the sake of brevity) one obtains

$$\det g = \left(1 + \sum_{p=1}^{m} (f^p_{x^1})^2 + (f^p_{x^2})^2 + (f^p_{x^3})^2\right) \det \tilde{g}, \tag{8}$$

where $\tilde{g}$ is the metric established by the transformation $\tilde{\mathbf{x}}(\boldsymbol{\xi}) : \mathbb{R}^3 \to \mathbb{R}^3$ of the parametric cube $\mathcal{P}$ onto the physical domain Ω. The Jacobian (determinant of the Jacobian matrix) of this mapping is

$$\sqrt{\det \tilde{g}} = \tilde{\mathbf{r}}_{\xi^1} \cdot (\tilde{\mathbf{r}}_{\xi^2} \times \tilde{\mathbf{r}}_{\xi^3}),$$

where $\tilde{\mathbf{r}} = (x^1, x^2, x^3)$ and the expression on the right-hand side is a triple scalar product.

Substituting (8) in (3) gives the final form of the functional to be used in calculations,

$$\mathcal{D} = \frac{1}{3^{3/2}} \int_0^1 \int_0^1 \int_0^1 \frac{(\mathrm{tr}(G^{-1}g))^{3/2}\sqrt{\det G}}{\sqrt{\det g}\sqrt{1+\sum_{p=1}^{m}(f^p_{x^1})^2+(f^p_{x^2})^2+(f^p_{x^3})^2}}\, \mathrm{d}\xi^1\, \mathrm{d}\xi^2\, \mathrm{d}\xi^3. \tag{9}$$

For a non-adaptive mesh construction, (9) turns to the functional employed for hexahedral mesh generation in [28]. That functional is universal, because an arbitrary given homeomorphic smooth mapping $\tilde{\mathbf{x}}(\boldsymbol{\xi})$ may be reproduced by minimizing the functional with a given metric G. In other words, an arbitrary given non-folded mesh may be reproduced by using this functional. One may ask the question: What is the sense of constructing a mapping if it is already given? To give an answer, we consider the following example. Let a parametric domain $\mathcal{P} \subset \mathbb{R}^3$ and a physical domain $\Omega \subset \mathbb{R}^3$ consist of two subdomains $\mathcal{P} = \mathcal{P}_1 \cup \mathcal{P}_2$ and $\Omega = \Omega_1 \cup \Omega_2$, and the mapping $\tilde{\mathbf{x}}_1(\boldsymbol{\xi}) : \mathcal{P}_1 \to \Omega_1$ be given. It is required to find a mapping $\tilde{\mathbf{x}}_2(\boldsymbol{\xi}) : \mathcal{P}_2 \to \Omega_2$ so that it is a smooth extension of $\tilde{\mathbf{x}}_1(\boldsymbol{\xi})$. If to implement a method with this aim (to use a functional, differential equations, etc.), then these two different mappings $\tilde{\mathbf{x}}_1(\boldsymbol{\xi})$ and $\tilde{\mathbf{x}}_2(\boldsymbol{\xi})$ should be smoothly conjugated. This is an additional and not easy problem. At the discrete level of mesh construction, it implies that the grid is given in Ω_1 and it is required to extend it smoothly into Ω_2. In other words, the mesh consists of two blocks and on their joint boundary the coordinate lines should be smoothly conjugated. In the present method, both the mappings $\tilde{\mathbf{x}}_1(\boldsymbol{\xi})$ and $\tilde{\mathbf{x}}_2(\boldsymbol{\xi})$ are defined within a common approach, i.e., using the same functional. Hence, the mapping $\mathbf{x}_1(\boldsymbol{\xi})$ may be smoothly extended to $\tilde{\mathbf{x}}_2(\boldsymbol{\xi})$ by varying gradually the metric elements G_{ij} in the vicinity of the boundary between Ω_1 and Ω_2. For instance, this feature allows the orthogonalization and condensation of the mesh near the body so as to resolve the boundary layers in viscous flow problems [28], or to construct a mesh in unsteady problems when the boundary of the physical domain Ω moves rapidly [31,32,35]. In Section 10, it is employed to improve mesh quality. G is called a control metric, since it allows for additional control over the mesh coordinatesurfaces. The absolute minimum of $\mathcal{D}$ is equal to 1, but it is rarely attained, except in simple domains or when a given mesh is reproduced with given elements G_{ij}.

For the case $n = 2$ with $\tilde{\mathbf{x}} = (x, y)$ and $\boldsymbol{\xi} = (\xi, \eta)$, from (2) and formulae for the monitor metric g, analogous to (4), (6), (7), when the control metric G is Euclidian, one obtains the functional proposed in [18],

$$\mathcal{D} = \frac{1}{2} \int_0^1 \int_0^1 \frac{\alpha_{11}(x_\xi^2 + x_\eta^2) + 2\alpha_{12}(x_\xi y_\xi + x_\eta y_\eta) + \alpha_{22}(y_\xi^2 + y_\eta^2)}{(x_\xi y_\eta - x_\eta y_\xi)\sqrt{1+\sum_{p=1}^{m}(f^p_x)^2+(f^p_y)^2}}\, \mathrm{d}\xi\, \mathrm{d}\eta. \tag{10}$$

If a scalar monitor function is used, then (10) becomes a functional proposed in [15], and its minimizer employs the mapping $\mathcal{P} \to \mathcal{M}$ of the parametric square $0 \leqslant \xi,\ \eta \leqslant 1$ onto the monitor surface $z = f(x, y)$ in space x, y, f. This mapping is inverse of the harmonic mapping $\mathcal{M} \to \mathcal{P}$. The harmonic mapping $\mathcal{M} \to \mathcal{P}$ exists and is a diffeomorphism (cf. [36]). The functional (10) with a vector-valued or scalar monitor function was employed for adaptive grid generation in [3,17–20,22,23] and others.

4. Non-degeneracy conditions for the mesh

Let us consider non-degeneracy conditions for a 3-D mesh produced by the mapping $\tilde{\mathbf{x}}(\boldsymbol{\xi}) : \mathcal{P} \to \Omega$, since, when adapting, the grid is actually sought in Ω. We use the definition of the non-folded mesh, which is quite close to the one given in [33].

Definition 1. A non-folded mesh is one which does not contain folded or self-intersecting cells, self-intersecting coordinate lines and surfaces, or coincident cells or nodes, and in most cases the Jacobian of the mapping $J = \det \tilde{\mathbf{x}}'(\boldsymbol{\xi}) > 0$ everywhere in $\mathcal{P}$.

Thus, the grid generation task (including adaptivity) is to find a homeomorphic mapping $\mathcal{P} \to \Omega$ subject to a specified homeomorphism $\partial\mathcal{P} \to \partial\Omega$ and a non-folded mesh (e.g., cubic one) is given in $\mathcal{P}$. The requirement $J > 0$ is necessary to construct a non-degenerate curvilinear coordinate system in Ω. However, there is an

exception when $J = 0$ on a subset of a lower dimension (e.g., isolated points, curves or surfaces in $\mathcal{P}$). Homeomorphism of the mapping is retained and cells may be still called non-folded if they are admissible for physical modeling. As an example we may point out the prismatic cell (cf. [28,33]) when $J = 0$ on the cell edge.

It is still an open question concerning conditions under which the mapping $\tilde{\mathbf{x}}(\boldsymbol{\xi})$, specified by the minimizer of (9), is a homeomorphism. It was suggested in [37], that sufficient conditions were for the mapping to be a global homeomorphism with the use of only local information about the mapping and its properties on the boundaries of both image and pre-image. They may be applied to provide non-degeneracy of a mesh. Note that, in the present method, the mesh is generated by employing a continuous piecewise smooth transformation, i.e., composed of smooth mappings $\tilde{\mathbf{x}}_i(\boldsymbol{\xi})$ of every grid element (cell) $\mathcal{P}_i$ in the domain $\mathcal{P}$ to a corresponding element Ω_i in Ω.

Let $\mathcal{P}, \Omega$ be bounded connected domains in $\mathbb{R}^n$ and $\overline{\mathcal{P}}, \overline{\Omega}$ be their diffeomorphic closures. Let $\mathbf{x}(\boldsymbol{\xi}) : \overline{\mathcal{P}} \to \overline{\Omega}$ be a $\mathbb{C}^1$ mapping. The following statement is valid (Theorem 4 of [37]).

Theorem 1. *Let* $\mathbf{x}(\boldsymbol{\xi})$ *map homeomorphically* $\partial\mathcal{P}$ *onto* $\partial\Omega$ *and the Jacobian of the mapping*

$$J = \det \mathbf{x}'(\boldsymbol{\xi}) > 0, \quad \boldsymbol{\xi} \in \overline{\mathcal{P}}.$$

Then $\mathbf{x}(\boldsymbol{\xi})$ *is a homeomorphism from* $\overline{\mathcal{P}}$ *onto* $\overline{\Omega}$.

Remark. It is worth noting that in [38], the analogous statement for the cases $n = 2, 3$ was proved in Lemmas 10.3.5 and 10.4.2 under the additional condition that $\overline{\mathcal{P}} \to \overline{\Omega}$ is a surjective transformation.

The homeomorphicity conditions of a continuous mapping have also been established (Theorem 6 of [37]).

Theorem 2. *Let* $\mathbf{x}(\boldsymbol{\xi})$ *map homeomorphically* $\partial\mathcal{P}$ *onto* $\partial\Omega$ *and be a local homeomorphism from* $\overline{\mathcal{P}}$ *onto* $\overline{\Omega}$ (*homeomorphism in the vicinity of any point of* $\overline{\mathcal{P}}$). *Then* $\mathbf{x}(\boldsymbol{\xi})$ *is a homeomorphism from* $\overline{\mathcal{P}}$ *onto* $\overline{\Omega}$.

Let $\mathcal{P}$ be partitioned into nonintersecting subdomains $\mathcal{P}_i$, $i = 1, \ldots, m$,

$$\overline{\mathcal{P}} = \bigcup_{i=1}^{m} \overline{\mathcal{P}_i}.$$

Let $\mathbf{x}(\boldsymbol{\xi}) : \overline{\mathcal{P}} \to \overline{\Omega}$ be a continuous mapping, being a $\mathbb{C}^1$ mapping on closures $\overline{\mathcal{P}_i}$. Denote the restriction of $\mathbf{x}(\boldsymbol{\xi})$ onto $\overline{\mathcal{P}_i}$ by $\mathbf{x}_i(\boldsymbol{\xi})$. Theorems 1 and 2 have, as a consequence, the following property (Theorem 9 of [37]).

Theorem 3. *Let* $\mathbf{x}(\boldsymbol{\xi})$ *map homeomorphically* $\partial\mathcal{P}$ *onto* $\partial\Omega$, *its restriction* $\mathbf{x}_i(\boldsymbol{\xi})$ *map homeomorphically* $\partial\mathcal{P}_i$ *onto* $\mathbf{x}_i(\partial\mathcal{P}_i)$ *for any* $i = 1, \ldots, m$, *and*

$$J_i = \det \mathbf{x}_i'(\boldsymbol{\xi}) > 0, \quad \boldsymbol{\xi} \in \overline{\mathcal{P}_i}, \ i = 1, \ldots, m.$$

Then $\mathbf{x}(\boldsymbol{\xi})$ *is a homeomorphism from* $\overline{\mathcal{P}}$ *onto* $\overline{\Omega}$.

Theorem 3 can be applied to obtain sufficient non-degeneracy conditions for a grid, for instance a hexahedral mesh. Let $\mathcal{P}$ be the parametric domain and Ω be the physical domain in $\mathbb{R}^3$. Given the homeomorphism $\partial\mathcal{P} \to \partial\Omega$, if for each grid element $\mathcal{P}_i$ (cube) in $\mathcal{P}$ its boundary $\partial\mathcal{P}_i$ is mapped homeomorphically by $\tilde{\mathbf{x}}_i(\boldsymbol{\xi})$ onto the boundary $\partial\Omega_i$ of the grid element Ω_i (hexahedron) in Ω, and for all elements $\det \tilde{\mathbf{x}}_i'(\boldsymbol{\xi}) > 0$, $\boldsymbol{\xi} \in \overline{\mathcal{P}_i}$, then by Theorem 3 the global piecewise smooth mapping $\tilde{\mathbf{x}}(\boldsymbol{\xi})$ is a homeomorphism. Hence, we need conditions of positivity for the Jacobian J_i of the mapping of the cube $\mathcal{P}_i$ onto the hexahedron Ω_i, since the homeomorphism $\partial\mathcal{P}_i \to \partial\Omega_i$ is assumed given. This issue is discussed in Section 5.

5. Non-degeneracy conditions for a cell

In this paper, we consider grids composed of hex cells. As noted in Section 4, non-degeneracy of a mesh implies that its every cell is non-folded (given by a homeomorphic mapping). Consider a hex cell in space x^1, x^2, x^3, see Fig. 3a, which is specified via the trilinear transformation of the unit cube $I^3 = \{(\xi^1, \xi^2, \xi^3): 0 \leqslant \xi^1, \xi^2, \xi^3 \leqslant 1\}$ from parametric space,

$$\tilde{\mathbf{r}} = \mathbf{w}_1 + \mathbf{w}_2\xi^1 + \mathbf{w}_4\xi^2 + \mathbf{w}_5\xi^3 + \mathbf{w}_3\xi^1\xi^2 + \mathbf{w}_6\xi^1\xi^3 + \mathbf{w}_8\xi^2\xi^3 + \mathbf{w}_7\xi^1\xi^2\xi^3, \tag{11}$$

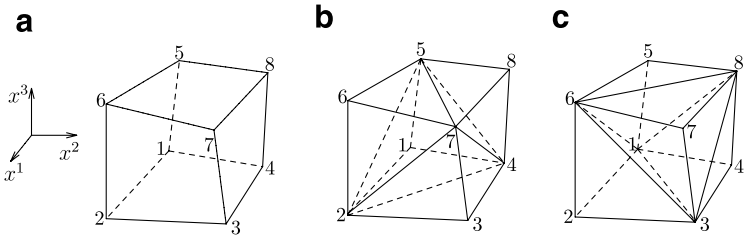

Fig. 3. Hex cell (a) and 2 dodecahedra (b), (c) with planar triangular faces. The first dodecahedron (b) is decomposed into 4 corner tetrahedra, $T_{1245}, T_{3427}, T_{6572}, T_{8754}$, and internal T_{2457}. The second one (c) is decomposed into 4 corner tetrahedra, $T_{2316}, T_{4138}, T_{5861}, T_{7683}$, and internal T_{1386}.

where the vectors $\mathbf{w}_i$ are

$$\mathbf{w}_1 = \tilde{\mathbf{r}}_1, \quad \mathbf{w}_2 = \tilde{\mathbf{r}}_2 - \tilde{\mathbf{r}}_1, \quad \mathbf{w}_3 = \tilde{\mathbf{r}}_3 - \tilde{\mathbf{r}}_2 - \tilde{\mathbf{r}}_4 + \tilde{\mathbf{r}}_1, \quad \mathbf{w}_4 = \tilde{\mathbf{r}}_4 - \tilde{\mathbf{r}}_1, \quad \mathbf{w}_5 = \tilde{\mathbf{r}}_5 - \tilde{\mathbf{r}}_1,$$
$$\mathbf{w}_6 = \tilde{\mathbf{r}}_6 - \tilde{\mathbf{r}}_2 - \tilde{\mathbf{r}}_5 + \tilde{\mathbf{r}}_1, \quad \mathbf{w}_7 = \tilde{\mathbf{r}}_7 - \tilde{\mathbf{r}}_3 - \tilde{\mathbf{r}}_6 - \tilde{\mathbf{r}}_8 + \tilde{\mathbf{r}}_2 + \tilde{\mathbf{r}}_4 + \tilde{\mathbf{r}}_5 - \tilde{\mathbf{r}}_1, \quad \mathbf{w}_8 = \tilde{\mathbf{r}}_8 - \tilde{\mathbf{r}}_4 - \tilde{\mathbf{r}}_2 + \tilde{\mathbf{r}}_1,$$

and $\tilde{\mathbf{r}}_i = (x^1, x^2, x^3)_i$ are the coordinates of the cell vertex. In general, a hex cell has non-planar faces, being the ruled surfaces of the second order.

Hence, for a hex cell to be non-folded, it is sufficient that the Jacobian of the mapping (11)

$$J = \tilde{\mathbf{r}}_{\xi^1} \cdot (\tilde{\mathbf{r}}_{\xi^2} \times \tilde{\mathbf{r}}_{\xi^3})$$

is positive everywhere in the cell, subject to the given boundary correspondence. J is a polynomial of fourth degree depending on three variables ξ^1, ξ^2, ξ^3 (with a maximum of second degree of each) [34]. There is, as yet, no known necessary and sufficient condition which can be used to say definitely whether a hex cell is inverted or not [33,34].

In [28], instead of a hex cell it was proposed to consider 2 dodecahedra of the first and second type (see Fig. 3b and c) spanned by the same vertices. Each dodecahedron is decomposed into the 5 tetrahedra: 4 corner ones and 1 internal. The trilinear mapping (11) is replaced by the set of linear transformations $\tilde{\mathbf{r}}^h(\boldsymbol{\xi})$ of the basic tetrahedra in parametric space to corresponding tetrahedra composing 2 dodecahedra in space x^1, x^2, x^3. The unit cube in Fig. 4a is partitioned into the 5 basic tetrahedra by two ways likewise in Fig. 3b,c. One of the 8 corner tetrahedra is shown in Fig. 4b, and one of the 2 internal tetrahedra is shown in Fig. 4c. When constructing the mesh, we ensure non-degeneracy of the 10 tetrahedra composing the first and second dodecahedra for every hex cell. Thus, the non-degeneracy condition for two grids composed of dodecahedral cells of the first or second type may be written in the form of inequalities

$$[V_m]_n > 0, \quad m = 1, \ldots, 10, \ n = 1, \ldots, N_c, \tag{12}$$

where V_m is the algebraic volume of the mth tetrahedron in the nth cell, and N_c is the number of the hex cells. This condition may be rewritten in terms of J_m for the linear transformation of the basic tetrahedron since

$$J_m = 6V_m. \tag{13}$$

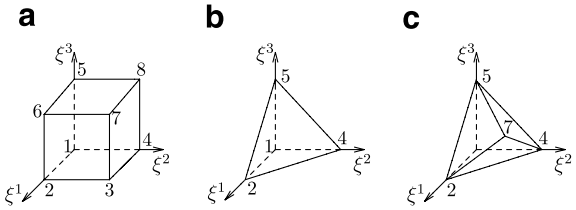

Fig. 4. In parametric space, unit cube (a) is partitioned into 5 basic tetrahedra: 4 corner ones, like T_{1245} (b), and internal T_{2457} (c). Two such partitions are employed (see Fig. 3b and c).

The sets of non-folded hex and dodecahedral cells do not coincide. The study of this issue was executed in [28]. For a non-folded hex cell, one or both corresponding dodecahedra may be inverted. Conversely, one may locate the vertices of an individual cell so that both dodecahedra are non-folded and the hex cell is folded. Nevertheless, practical implementation has shown that if the condition (12) is satisfied, then the hexahedral grid is non-folded. For the final verification of hexahedral grid non-degeneracy, we apply, first, the sufficient condition 2 for a hex cell to be non-folded of [34] and next, for the cells not satisfying it, the necessary condition NC4 of [28] is checked. In the former, 27 inequalities combining the volumes of 32 tetrahedra are checked. In the latter, one examines the sign of the Jacobian of (11) in the segments joining the points on the opposite cell faces.

6. Discretization of functional

In Section 3, it is noted that in the 2-D case the harmonic mapping $\mathcal{M} \to \mathcal{P}$ exists and is a diffeomorphism. The inverse mapping $\mathcal{P} \to \mathcal{M}$ is constructed by minimizing the functional (10). Numerical practice has shown that, when seeking a discrete mapping using elliptic partial differential equations for the physical domain Ω of complicated geometry (e.g., non-convex Ω with sharp inward corners on $\partial\Omega$), the one-to-one nature of the inverse mapping may be lost. As an example we refer to non-adaptive grid construction for the backward facing step domain (see, [23, pp. 8–36]). By Radó's theorem (see e.g. [39]) the harmonic mapping of the simply connected bounded domain Ω onto the analogous convex domain $\mathcal{P}$ (say, parametric square), subject to a given homeomorphism $\partial\Omega \to \partial\mathcal{P}$, is a diffeomorphism. However, the discrete implementation of the inverse mapping $\mathcal{P} \to \Omega$ by Winslow's method [40] (using inverted Laplace's equations) produces meshes composed of quadrilateral cells with self-intersecting grid lines independently of whether a coarse or refined grid is constructed. In [25], a special way of discretizing the functional was proposed, known as a variational barrier method. It allows the construction of non-folded meshes in arbitrary 2-D domains.

The 3-D case is much harder. For the harmonic mapping, extension of Radó's theorem to the spatial case is not valid (see [41,42]). On the other hand, practical computations have shown that the class of homeomorphic piecewise smooth mappings is not empty, even when Ω involves complicated geometry. As shown in Section 4, for the grid to be non-folded, each one of its cells should be non-folded. The barrier property of the discrete functional plays a substantial role in obtaining a non-folded mesh.

Let a structured mesh of $N_1 \times N_2 \times N_3$ nodes be generated in a domain Ω. For convenience, instead of the unit cube in parametric space we consider the rectangular parallelepiped with edges $N_1 - 1, N_2 - 1, N_3 - 1$. In each of the $N_c = (N_1 - 1)(N_2 - 1)(N_3 - 1)$ cells, the functional (9) is discretized by averaging its approximation over the 10 basic tetrahedra. The resulting difference function (or discrete functional) is

$$\mathcal{D}^h = \frac{1}{N_c} \sum_{n=1}^{N_c} \sum_{m=1}^{10} \frac{1}{10} [E_m]_n, \tag{14}$$

where $[E_m]_n$ is the integrand in (9) computed for the mth tetrahedron in the nth cell.

If the set of non-folded grids composed of dodecahedral cells is not empty the system of the algebraic equations written for the internal nodes,

$$R_{x^i} = \frac{\partial \mathcal{D}^h}{\partial x_n^i} = 0, \quad i = 1, 2, 3, \tag{15}$$

has at least one solution which corresponds to a non-folded mesh. Here n is a global node number. To find this solution, we apply unconstrained minimization taking a non-folded grid as an initial guess. For the initial folded grid, an untangling procedure is considered in [28]. In [28], we have proved the following theorem:

Theorem 4. *The function $\mathcal{D}^h$ possesses an infinite barrier on the boundary of the set of non-folded grids composed of dodecahedral cells of the first or second type.*

The meaning of the barrier property is the following. Let, while grid nodes are moving, one of the 5 tetrahedra of the dodecahedral cell be close to degeneration, i.e., its volume V_m tends to zero while remaining positive. Recall that in (9) we have $\sqrt{\det \bar{g}} = J$. By virtue of (13), there is a value tending to zero in the

denominator of (14) in the corresponding term. Therefore, this term tends to infinity and $\mathcal{D}^h$ does as well. This is an infinite barrier preventing cell folding while minimizing $\mathcal{D}^h$. Hence, by Theorem 3 of Section 4, the two grids composed of dodecahedral cells of the first or second type are also non-folded and that, in turn, ensures non-degeneracy of the hexahedral mesh in practical computations.

For the first time in 3-D, the barrier property of the discrete functional was applied in [3,23], while the set of linear transformations of the 24 basic tetrahedra is employed for each hex cell.

7. Minimization procedure

The procedure of unconstrained minimization is applied to find a minimum of $\mathcal{D}^h$. Given a non-folded mesh at the lth iteration step, the coordinates of the nth grid node at the $l+1$th step are obtained by using the quasi-Newton procedure in the sense that in the Hessian only the diagonal elements are retained

$$\tau R_{x^i} + \sum_{j=1}^{3} R_{x^i x^j}\left((x_n^j)^{l+1} - (x_n^j)^l\right) = 0, \quad i = 1,2,3, \tag{16}$$

where $R_{x^i x^j} = \frac{\partial^2 \mathcal{D}^h}{\partial x_n^i \, \partial x_n^j}$ and $\tau < 1$ is the iterative parameter. The iterations are employed until the condition

$$\max_n |\tilde{\mathbf{r}}_n^{l+1} - \tilde{\mathbf{r}}_n^l| < \varepsilon$$

is satisfied. Here $\varepsilon > 0$ is sufficiently small. The experience of 2-D modeling on adaptive meshes has shown that bringing of the iterative process (16) to convergence requires too many mesh iterations. Hence, at every time step of an unsteady physical problem, one implements only a relatively small number of mesh iterations. This is especially justified, since after every mesh iteration one has to update again the physical parameters of the main problem at this time. Due to the infinite barrier, we can specify an iterative parameter τ that the mesh will remain non-folded in the course of computation.

To implement the minimization procedure (16), one should compute the first and second derivatives of $\mathcal{D}^h$. We will derive these formulae in the next section.

8. Computational formulae

Write the integrand of (9) in the form $E = U/V$, where

$$U = \gamma (G^{ij} g_{ji})^{3/2}, \quad V = \sqrt{\det \tilde{g}} = \tilde{\mathbf{r}}_{\xi^1} \cdot (\tilde{\mathbf{r}}_{\xi^2} \times \tilde{\mathbf{r}}_{\xi^3}),$$
$$\gamma = 3^{-3/2}\sqrt{\det G}\left(1 + \sum_{p=1}^{m} (f_{x^1}^p)^2 + (f_{x^2}^p)^2 + (f_{x^3}^p)^2\right)^{-1/2}.$$

To obtain the derivatives, we utilize the chain rule

$$E_{x^i} = \frac{U_{x^i} - E V_{x^i}}{V}, \quad E_{x^i x^j} = \frac{U_{x^i x^j} - 2E_{x^i} V_{x^j} - E V_{x^i x^j}}{V}, \quad i,j = 1,2,3.$$

Differentiating the numerator U yields

$$U_{x^m} = \frac{3}{2}\gamma (G^{ij} g_{ji})^{1/2} G^{kl} \frac{\partial g_{lk}}{\partial x^m},$$
$$U_{x^m x^n} = \frac{3}{2}\gamma (G^{ij} g_{ji})^{-1/2}\left[\frac{1}{2} G^{ij} \frac{\partial g_{ji}}{\partial x^m} G^{kl} \frac{\partial g_{lk}}{\partial x^n} + G^{ij} g_{ji} G^{kl} \frac{\partial^2 g_{lk}}{\partial x^m \partial x^n}\right], \quad i,j,k,l,m,n = 1,2,3. \tag{17}$$

When differentiating, the derivatives $f_{x^i}^p$ are fixed, i.e., the metric is frozen. This issue is discussed in Section 11.

As noted in Section 6, the functional is discretized on the 10 tetrahedra. Consider the linear mapping $\mathbf{r}^h(\boldsymbol{\xi})$ which transforms the basic tetrahedron T_{1245} (see Fig. 4b) to the corresponding corner tetrahedron T_{1245} of a dodecahedral cell in $\mathcal{M}$. Meanwhile, the linear mapping $\tilde{\mathbf{r}}^h(\boldsymbol{\xi})$, transforming this basic tetrahedron to the corner tetrahedron T_{1245} of a dodecahedral cell in space x^1, x^2, x^3 (see Fig. 3b), is

$$\tilde{\mathbf{r}}^h = (\tilde{\mathbf{r}}_2 - \tilde{\mathbf{r}}_1)\xi^1 + (\tilde{\mathbf{r}}_4 - \tilde{\mathbf{r}}_1)\xi^2 + (\tilde{\mathbf{r}}_5 - \tilde{\mathbf{r}}_1)\xi^3 + \tilde{\mathbf{r}}_1, \quad 0 \leqslant \xi^1, \xi^2, \xi^3;\ \xi^1 + \xi^2 + \xi^3 \leqslant 1.$$

Substituting the derivatives $\tilde{\mathbf{r}}^h_{\xi^i}$ in (6) gives the formulae for the metric elements g_{ij}

$$g_{11} = \alpha_{kl}(x_2^k - x_1^k)(x_2^l - x_1^l), \quad g_{22} = \alpha_{kl}(x_4^k - x_1^k)(x_4^l - x_1^l), \quad g_{33} = \alpha_{kl}(x_5^k - x_1^k)(x_5^l - x_1^l),$$
$$g_{12} = \alpha_{kl}(x_2^k - x_1^k)(x_4^l - x_1^l), \quad g_{13} = \alpha_{kl}(x_2^k - x_1^k)(x_5^l - x_1^l), \quad g_{23} = \alpha_{kl}(x_2^k - x_1^k)(x_5^l - x_1^l),$$

$k, l = 1, 2, 3$. The coefficients α_{ij} are defined by (7) and the nodal values of the finite difference approximations to the derivatives $(f^p_{x^k})^h$ are required. $(f^p_{x^k})^h$ will be calculated below.

When computing the derivatives of U, in (17) we replace x^k by x_i^k, where i is the vertex number in T_{1245}. For instance, at the vertex 1, the derivatives of g_{11} with respect to x_1^k are

$$\frac{\partial g_{11}}{\partial x_1^k} = 2\alpha_{kl}(x_1^l - x_2^l), \quad \frac{\partial^2 g_{11}}{\partial (x_1^k)^2} = 2\alpha_{kk}, \quad l = 1, 2, 3.$$

Other derivatives and derivatives at the vertices $i = 2, 4, 5$ are obtained in a similar spirit. The derivatives of the denominator V are given in [28, p. 731]. The integrand in (9) is invariant to rotation of the coordinate system $\boldsymbol{\xi}$, therefore, these formulae may be applied to the other 7 corner tetrahedra after a proper substitution of the vertex number.

Next consider the linear mapping $\mathbf{r}^h(\boldsymbol{\xi})$ which transforms the basic tetrahedron T_{2457} (see Fig. 4c) to the corresponding internal tetrahedron T_{2457} of a dodecahedral cell in $\mathcal{M}$. Meanwhile, the linear mapping $\tilde{\mathbf{r}}^h(\boldsymbol{\xi})$, transforming this basic tetrahedron to the internal tetrahedron T_{2457} of a dodecahedral cell in space x^1, x^2, x^3 (see Fig. 3c), is

$$\tilde{\mathbf{r}}^h = \frac{1}{2}(\tilde{\mathbf{r}}_7 + \tilde{\mathbf{r}}_2 - \tilde{\mathbf{r}}_4 - \tilde{\mathbf{r}}_5)\xi^1 + \frac{1}{2}(\tilde{\mathbf{r}}_7 + \tilde{\mathbf{r}}_4 - \tilde{\mathbf{r}}_2 - \tilde{\mathbf{r}}_5)\xi^2 + \frac{1}{2}(\tilde{\mathbf{r}}_7 + \tilde{\mathbf{r}}_5 - \tilde{\mathbf{r}}_2 - \tilde{\mathbf{r}}_1)\xi^3 + \frac{1}{2}(\tilde{\mathbf{r}}_2 + \tilde{\mathbf{r}}_4 + \tilde{\mathbf{r}}_5 - \tilde{\mathbf{r}}_7),$$
$$0 \leqslant \xi^1, \xi^2, \xi^3;\ \xi^1 + \xi^2 + \xi^3 \leqslant 1.$$

Substituting the derivatives $\tilde{\mathbf{r}}^h_{\xi^i}$ in (6) gives the formulae for the metric elements g_{ij}

$$g_{11} = \frac{1}{4}\alpha_{kl}(x_7^k + x_2^k - x_5^k - x_4^k)(x_7^l + x_2^l - x_5^l - x_4^l), \quad g_{22} = \frac{1}{4}\alpha_{kl}(x_7^k + x_4^k - x_5^k - x_2^k)(x_7^l + x_4^l - x_5^l - x_2^l),$$
$$g_{33} = \frac{1}{4}\alpha_{kl}(x_7^k + x_5^k - x_2^k - x_4^k)(x_7^l + x_2^l - x_5^l - x_4^l), \quad g_{12} = \frac{1}{4}\alpha_{kl}(x_7^k + x_2^k - x_5^k - x_4^k)(x_7^l + x_4^l - x_5^l - x_2^l),$$
$$g_{13} = \frac{1}{4}\alpha_{kl}(x_7^k + x_2^k - x_5^k - x_4^k)(x_7^l + x_2^l - x_5^l - x_4^l), \quad g_{23} = \frac{1}{4}\alpha_{kl}(x_7^k + x_4^k - x_5^k - x_2^k)(x_7^l + x_2^l - x_5^l - x_4^l),$$

$k, l = 1, 2, 3$.

When computing the derivatives of U, in (17) we replace x^k by x_i^k. For instance, at the vertex 2, the derivatives of g_{11} with respect to x_2^k are

$$\frac{\partial g_{11}}{\partial x_2^k} = \frac{1}{2}\alpha_{kl}(x_7^l + x_2^l - x_5^l - x_4^l), \quad \frac{\partial^2 g_{11}}{\partial (x_2^k)^2} = \frac{1}{2}\alpha_{kk}, \quad l = 1, 2, 3.$$

Other derivatives and derivatives at the vertices $i = 4, 5, 7$ are obtained in a similar spirit. The derivatives of the denominator V are given in [28, p. 733]. These formulae may be applied to the second internal tetrahedron T_{1368} after a proper substitution of the vertex number.

It is necessary to determine the nodal derivatives $f^h_{x^i}$ (for brevity, the superscript p is omitted implying that f is a scalar function) at the nodes. To this end, we resolve the system (5) about these derivatives

$$f_{x^i} = \tilde{b}^{-1}_{ij} f_{\xi^j}, \quad i, j = 1, 2, 3, \tag{18}$$

where $\tilde{b}^{-1}$ is the inverse matrix for the Jacobian matrix $\partial x^i / \partial \xi^j$ of the mapping $\mathcal{P} \to \Omega$. In T_{1245}, the discrete derivative, denoted by $(f^h_{x^i})_1$, is calculated via the system (18), using the approximations

$$(x^i_{\xi^1})^h = x^i_2 - x^i_1, \quad (x^i_{\xi^2})^h = x^i_4 - x^i_1, \quad (x^i_{\xi^3})^h = x^i_5 - x^i_1, \quad i = 1,2,3, \quad f^h_{\xi^1} = f_2 - f_1, \quad f^h_{\xi^2} = f_4 - f_1,$$
$$f^h_{\xi^3} = f_5 - f_1.$$

Next the nodal derivative $f^h_{x^i}$ is interpolated through the values of $(f^h_{x^i})_l$ in the 8 corner tetrahedra, adjacent to the underlying node,

$$f^h_{x^i} = \sum_{l=1}^{8} (f^h_{x^i})_l V_l \left(\sum_{l=1}^{8} V_l \right)^{-1},$$

where V_l is the tetrahedron volume. Due to (13), instead of V_l one may use the Jacobian J_l of the linear transformation, and it abridges computations because one uses J_l when solving the system (18).

If the monitor function is given in the cell center, one should update it at the grid nodes.

We apply an additional parameter, the adaptive coefficient c_a, to control the number of grid nodes lying in the layer of high gradients of the component f^p. The greater c_a is, the higher the relative number of grid nodes in the layer of high gradients is. To this end, instead of f^p one should substitute $c_a f^p$. In addition, each f^p is scaled so that the difference of the maximal and minimal values of f^p equals the diagonal of the rectangular parallelepiped circumscribed about the physical domain Ω, i.e.,

$$f^p_{\max} - f^p_{\min} = \sqrt{\sum_{j=1}^{3} (x^j_{\max} - x^j_{\min})^2}, \quad p = 1, \ldots, m.$$

Given the value of E and its derivatives at the vertices of the 10 tetrahedra, we form the elements of the system for the procedure (16). Let the local vertex numbers $1,2,\ldots,8$ in the cell correspond to the global grid node numbers $n_1, n_2, \ldots, n_8$. Then the value of E and its derivatives at the vertex 1 of T_{1245} are added to $\mathcal{D}^h$ and elements of the system (16)

$$\mathcal{D}^h = \mathcal{D}^h + E, \quad [R_{x^i}]_{n_1} = [R_{x^i}]_{n_1} + E_{x^i}, \quad [R_{x^i x^j}]_{n_1} = [R_{x^i x^j}]_{n_1} + E_{x^i x^j}, \quad i,j = 1,2,3.$$

We employ a notation drawn in programming languages. It implies, for instance, that a new value of $\mathcal{D}^h$ is equal to $\mathcal{D}^h + E$. The values at the vertices $2,4,5$ are added to $\mathcal{D}^h$ and corresponding elements $[R_{x^i}]_{n_2}, [R_{x^i x^j}]_{n_2}, [R_{x^i}]_{n_4}, [R_{x^i x^j}]_{n_4}, [R_{x^i}]_{n_5}, [R_{x^i x^j}]_{n_5}$. We treat E and its derivatives calculated at the vertices of the 9 remaining tetrahedra in a similar manner.

The method can be extended to unstructured grids in a straightforward manner. One needs only to define a correspondence between a local vertex number in a cell and a global grid node number.

9. Boundary nodes redistribution

If when modeling a physical problem, the boundary of the physical domain Ω moves and its shape changes substantially, it is necessary to redistribute the mesh nodes over the boundary $\partial\Omega$. Motion of the nodes inside Ω and on $\partial\Omega$ should be executed in a coordinated manner. When the monitor function suffers discontinuity (e.g. shocks approaching $\partial\Omega$), uncoordinated redistribution of the interior and boundary nodes (when, for example, it is executed using 3-D and 2-D functionals, respectively) may result in instability in grid generation and degenerate cells near $\partial\Omega$.

In [28], an algorithm was suggested for redistributing the nodes on $\partial\Omega$. In that approach, the problem of constrained minimization of $\mathcal{D}^h$ was solved subject to constraints defining $\partial\Omega$. The following discrete functional is to be minimized

$$\mathcal{D}^h_1 = \frac{1}{N_c} \sum_{n=1}^{N_c} \sum_{m=1}^{10} \frac{1}{10} [E_m]_n + \sum_{\tilde{\mathbf{r}}_l \in \partial\Omega} \lambda_l Q(\tilde{\mathbf{r}}_l) = \mathcal{D}^h + \sum_{l \in \mathcal{L}} \lambda_l Q_l;$$

here the constraints $Q_l = Q(\tilde{\mathbf{r}}_l) = 0$ define $\partial\Omega$, λ_l are the Lagrange multipliers, and $\mathcal{L}$ is the set of the boundary nodes. Since the function $Q(\tilde{\mathbf{r}})$ is assumed piecewise differentiable, the difference function $\mathcal{D}^h_1$ holds the infinite barrier on the boundary of the set of non-folded grids composed of dodecahedral cells.

Now the system of algebraic equations, analogous to (15), will be supplemented with the constraints

$$R_{x^i} = \frac{\partial \mathcal{D}^h}{\partial x_n^i} + \lambda_n \frac{\partial Q_n}{\partial x_n^i} = 0, \quad i = 1,2,3,\ Q_n = 0;$$

here $\lambda_n = 0$ if $n \notin \mathcal{L}$ and constraints are defined for the boundary nodes $n \in \mathcal{L}$. The case when $\partial\Omega$ is defined parametrically is considered in [28].

10. Examples of mesh

10.1. Horseshoe domain

In x, y, z-space, the domain is obtained by rotating a horseshoe about the z-axis. It is bounded from below by the top half-sphere of radius $r = 1$ with the center at $(0,0,0)$ and plane $z = 0$, and from above by the surface which is swept by the top semi-ellipse $z > 0$

$$x^2/a^2 + z^2/b^2 = 1, \quad a = 2,\ b = 9,$$

rotated about the z-axis. In planar grid generation, this horseshoe domain was employed for the purpose of truncation error study in [43]. We generate a "regular" (structured) grid of $61 \times 61 \times 51$ nodes in the sense that it is not obtained as the result of rotation of a 2-D mesh about the z-axis (in contrast to the cylindrical mesh). A schematic view is depicted in Fig. 5, which shows the 4 bounding coordinate surfaces $i = 1, 61$, $j = 1, 61$, lying in the plane $z = 0$, and the projection of the surface $k = 1$ (half-sphere) onto this plane. Hex cells, adjoining the 4 bounding edges $i,j = 1$; $i = 1$, $j = 61$; $i = 61$, $j = 1$; and $i,j = 61$ are the triangular prisms. In a prismatic cell, the functional is discretized on 8 tetrahedra (see [28, p. 728] for detail).

First, a non-adaptive mesh is constructed by the method proposed in [28] (see the surface $i = 31$ in Fig. 6). The control metric G is specified so that the upper cells are not stretched. If G had been the Euclidian metric, the upper cells would be rather stretched. In Fig. 10 of [28], one can find an example of stretched cells and the way to specify G.

Two surfaces are given in space

$$z^1(x) = 3 - 5(x + 0.8)(x + 0.4)(x + 0.2), \quad z^2(y) = 3 - 5(y + 0.8)(y + 0.4)(y + 0.2),$$

defining the form of the layers of high gradients of $\mathbf{f}$. The components of the monitor function f^p, $p = 1,2$, are

$$f^p = \begin{cases} 1 & \text{if } z \geqslant z^p + \delta^p, \\ 0.5(z - z^p + \delta^p)/\delta^p & \text{if } |z - z^p| < \delta^p, \\ 0 & \text{if } z \leqslant z^p - \delta^p, \end{cases} \tag{19}$$

where $\delta^p = 0.02\sqrt{1 + (z^p/x^p)^2}$ and $x^1 = x$, $x^2 = y$. We define $c_a = 0.015$.

The metric G is specified to be equal to the metric g of the mesh in Fig. 6. In non-adaptive mesh generation, the metric G, defined in this way, results in the reproduction of the same grid, while the functional $\mathcal{D}^h$ attains the absolute minimum value of 1 [28]. Hence, when adapting, the functional value increases. While generating the non-adaptive mesh, we move the nodes on the bounding surfaces and edges. While adapting, we additionally move the 8 corner points of the domain along the circles of radii $r = 1$, $r = 2$ in the plane $z = 0$. The

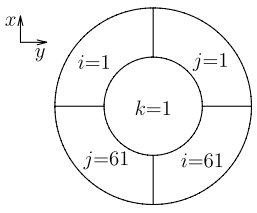

Fig. 5. Schematic view. Projection on the x,y-plane.

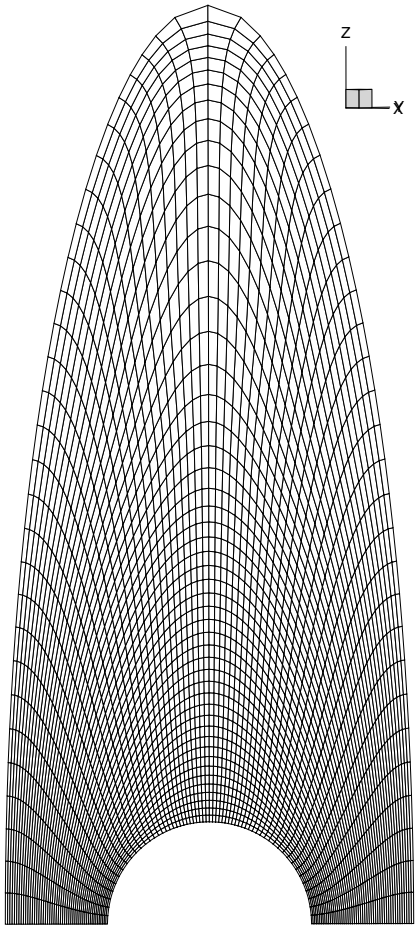

Fig. 6. Surface $i = 31$ of the non-adaptive mesh.

bottom view of the adapted mesh is presented in Fig. 7. The check of the hexahedral grid has shown that all hex cells are non-folded.

10.2. Interblade domain of turbine channel

An $81 \times 61 \times 41$ mesh is generated in the interblade domain of a turbine channel. Specifying the metric G provides mesh impaction towards the blades. A surface in the form $y(x)$, similar to that considered in Section 10.1, determines the form of the layer of high gradients. The scalar monitor function f is calculated by a formula similar to (19). The adapted mesh is shown in Fig. 8 and the fragment of the bounding surface $k = 41$ in Fig. 9. The check has shown that all hex cells are non-folded.

11. On singularity when adapting to discontinuous monitor function

For a model example, we consider a singularity appearing when adapting the mesh in hydrodynamical problems with discontinuous solution. In the denominator of (9) there are derivatives of the monitor function f (f is scalar). If f suffers a discontinuity across a certain surface, then, when grid nodes condense towards this surface, one of the derivatives, determined numerically, tends to infinity. This, in turn, causes the infinite barrier of $\mathcal{D}^h$ to disappear and mesh to fold. The mechanism for removing the barrier and the way to overcome this drawback is discussed in this section.

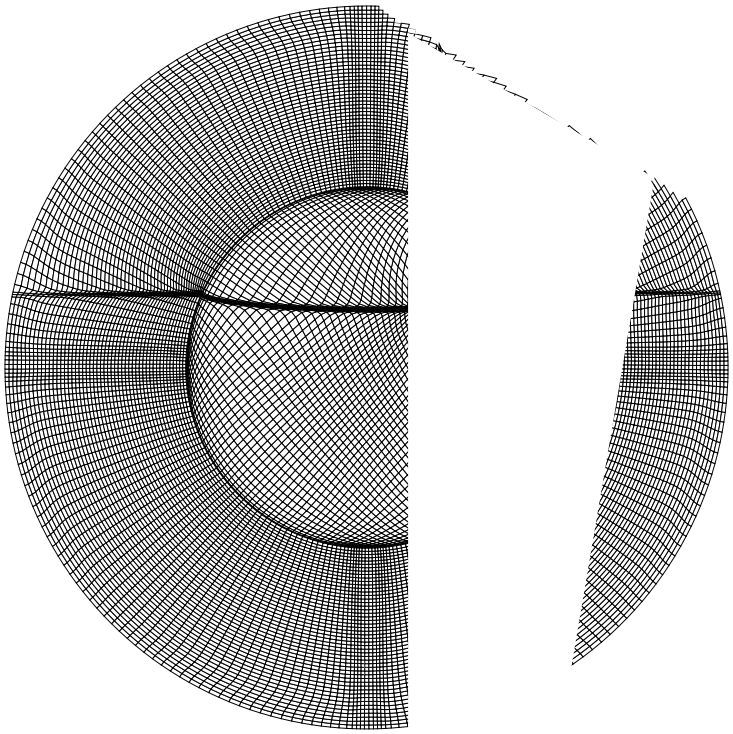

We analyze a discontinuous f when ıe nonlinear advection equation in one dimension, i.e., when the solution depends on one variable .e mesh is constructed in x, y, z-space using the functional (9). We solve the IVP given by the nonlin tion equation with discontinuous initial data, i.e.

$$\frac{\partial u}{\partial t} + u\frac{\partial u}{\partial x} = 0, \quad u(x,0) = \begin{cases} u_l \\ u_{\mathrm{r}} \end{cases} \quad). \qquad u_l > u_r > 0. \tag{20}$$

The shock moves from the left to righ speed $w = (u_l + u_{\mathrm{r}})/2$. In [19], the following case was shown. Let (1) this problem be solved by Godun heme on a 1-D moving mesh, (2) without adaptation, the grid nodes move with the speed w, (3) initi $t = 0$, the nodes be distributed uniformly and the midmesh node be at point $x = 0$. In this situation the erage values of the discrete function $u_{i+1/2}$ at the interval (x_i, x_{i+1}) center do not change with time when lated on the adaptive mesh.

It is sufficient to consider a grid of cells: two cells to the left of the discontinuity with $u_{i+1/2} = u_l$ and two cells to the right with $u_{i+1/2} = u_{\mathrm{r}}$. I o symmetry of the problem, we discuss only the two left cells. These cells are shown in Fig. 10 at the nth an + 1th time levels. Points 1 and 3 move with the speed w and point 2 shifts closer to 3 when adapting. We work in the frame moving with the speed w (see Fig. 11). In this frame, when minimizing the functiona points 1 and 3 are fixed and node 2 moves. Given $x_1 = 0$, one has $x_3 = L$, where $L = 2h$, h being the spac g of the initial uniform mesh. The coordinate x of point 2 is variable and determined while solving the varia onal problem. The nodal values of the function u_i are determined via the linear interpolation of $u_{i+1/2}$ and, herefore, $u_1 = u_2 = u_l$, $u_3 = (u_l + u_{\mathrm{r}})/2$. It is worth noting that points 1, 2, 3 are the nodes of a 3-D rectangu ar grid with uniform spacings in y, z and a certain number of nodes in these two directions.

Next consider discretization of the functional (9) on this grid. As a monitor function we apply u multiplied by the adaptive coefficient c_a. The manifold $\mathcal{M}$ is defined by the coordinates $\mathbf{x} = (x, y, z, c_a u)$, and domain $\mathcal{P}$ by

Fig. 8. Adaptive mesh in the interblade domain.

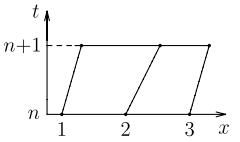

Fig. 10. Points 1,3 move with speed w, point 2 shifts towards 3 when adapting.

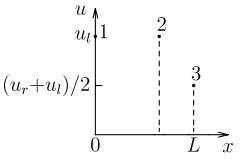

Fig. 11. In the moving frame, points 1,3 are fixed, coordinate x of point 2 is variable.

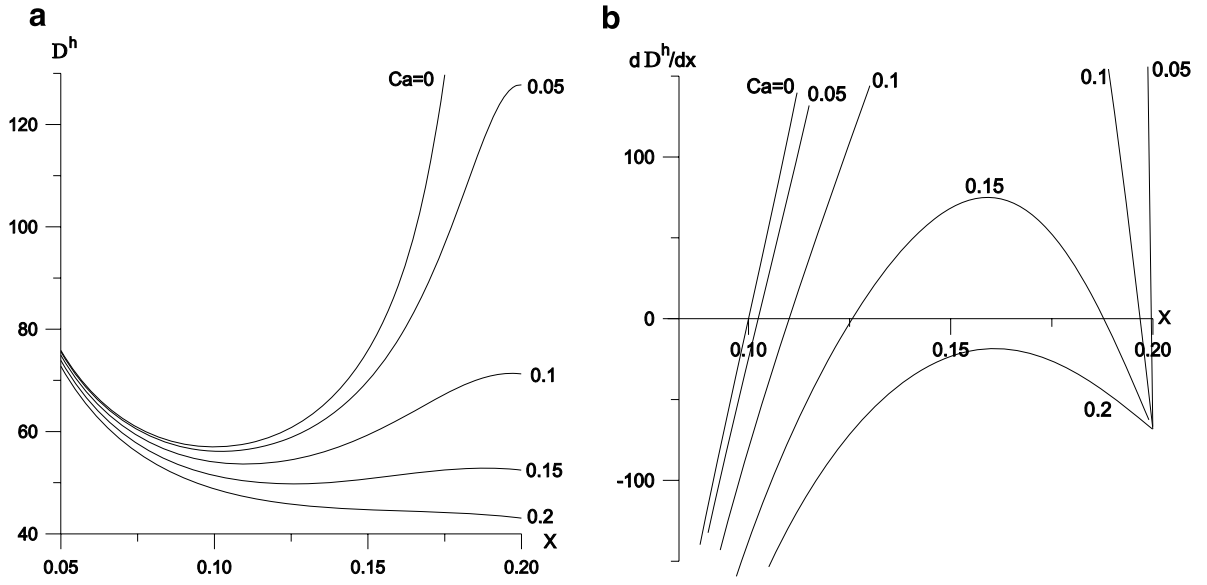

Fig. 12. Distributions of $\mathcal{D}^h$ (a) and $\partial\mathcal{D}^h/\partial x$ (b). With $c_a > 0$ $\mathcal{D}^h$ is not convex. With $c_a > c_a^{\mathrm{crt}}$ the minimum and maximum disappear (see curve $c_a = 0.2$ in (b)).

the coordinates $\boldsymbol{\xi} = (\xi, \eta, \zeta)$. The control metric G is Euclidian. The mapping $\mathcal{P} \to \Omega$ is defined by the functions $x = x(\xi)$, $y = a\eta$, $z = b\zeta$ (we assume that $a = b = 1$), and the metric elements are

$$g_{11} = x_\xi^2(1 + c_a^2 u_x^2), \quad g_{22} = 1, \quad g_{33} = 1, \quad g_{12} = g_{13} = g_{23} = 0.$$

For convenience, we omit the coefficient $3^{-3/2}$, so the functional (9) takes the form

$$\mathcal{D} = \int_0^1 \int_0^1 \int_0^1 \frac{(g_{11} + g_{22} + g_{33})^{3/2}}{\sqrt{\det \tilde{g}}\sqrt{1 + c_a^2 u_x^2}}\, \mathrm{d}\xi\, \mathrm{d}\eta\, \mathrm{d}\zeta = \int_0^1 \frac{[x_\xi^2(1 + c_a^2 u_x^2) + 2]^{3/2}}{x_\xi \sqrt{1 + c_a^2 u_x^2}}\, \mathrm{d}\xi.$$

This 1-D functional is calculated by the rectangular rule on the two-cell grid

$$\mathcal{D} = \sum_{i=1}^{2} \frac{[(x_\xi)_{i+1/2}^2(1 + c_a^2 (u_x)_{i+1/2}^2) + 2]^{3/2}}{(x_\xi)_{i+1/2}\sqrt{1 + c_a^2 (u_x)_{i+1/2}^2}} \Delta\xi_{i+1/2};$$

here the coefficient 0.5 at $\mathcal{D}^h$ is omitted for convenience, and the spacing is $\Delta\xi_{i+1/2} = \xi_{i+1} - \xi_i = 1$. Using a centered difference to approximate the derivatives

$$(x_\xi)_{i+1/2} = (x_{i+1} - x_i)/\Delta\xi_{i+1/2}, \quad (u_x)_{i+1/2} = (u_{i+1} - u_i)/(x_{i+1} - x_i),$$

we get, in the left and right cells,

$$(x_\xi)_{3/2} = x, \quad (u_x)_{3/2} = 0, \quad (x_\xi)_{5/2} = L - x, \quad c_a(u_x)_{5/2} = \beta/(L - x);$$

here $\beta = c_a|u_3 - u_2| = 0.5c_a|u_r - u_l|$. Then the discrete functional $\mathcal{D}^h$ is

$$\mathcal{D}^h = \frac{(x^2+2)^{3/2}}{x} + \frac{\left[(L-x)^2\left(1+\frac{\beta^2}{(L-x)^2}\right)+2\right]^{3/2}}{(L-x)\sqrt{1+\frac{\beta^2}{(L-x)^2}}}, \tag{21}$$

and its derivative is

$$\frac{\partial\mathcal{D}^h}{\partial x} = \frac{2\sqrt{x^2+2}(x^2-1)}{x^2} + \frac{2(L-x)\sqrt{(L-x)^2+\beta^2+2}}{[(L-x)^2+\beta^2]^{3/2}}[1-(L-x)^2-\beta^2]. \tag{22}$$

In Fig. 12, the distributions of $\mathcal{D}^h$ and $\partial\mathcal{D}^h/\partial x$ are presented for several values of c_a with $u_l = 2$, $u_r = 1$, initial unform spacing $h = 0.1$, and therefore, $\beta = 0.5c_a$. Behaviour of $\mathcal{D}^h$ is analogous to that in the 1-D and 2-D cases considered in [19]. With $c_a = 0$, $\mathcal{D}^h$ has a minimum at $x = 0.1$ which corresponds to the uniform grid. When $c_a > 0$, $\mathcal{D}^h$ loses convexity. There are a minimum and maximum (see Fig. 12b). Therefore, the solution of the problem of finding its extremum becomes non-unique. When increasing c_a, on one hand the minimum shifts to the right, corresponding to point 2 moving towards point 3, i.e., grid condensing. On the other hand, the maximum shifts to the left from point 3 causing grid rarefaction. In 3-D problems this may cause harsh node displacement due to jumps of the solution from the maximum to the minimum and vice versa during iterations and, therefore, grid surfaces may overlap. Furthermore, with a certain critical value c_a^{crt}, both extrema merge and further, when c_a increases further, they disappear (see the curve $c_a = 0.2$ in Fig. 12b). When $c_a > c_a^{\mathrm{crt}}$ there is no extremum and minimization of $\mathcal{D}^h$ causes the right cell to collapse.

Now, when differentiating $\mathcal{D}^h$, the metric is frozen, in other words the derivative u_x is assumed to not depend on x. The derivative of the new functional, fixing $\beta/(L-x)$ in (21), is found to be

$$\frac{\partial\mathcal{D}_1^h}{\partial x} = \frac{2\sqrt{x^2+2}(x^2-1)}{x^2} + \frac{2(L-x)\sqrt{(L-x)^2+\beta^2+2}}{(L-x)\sqrt{(L-x)^2+\beta^2}}(1-(L-x)^2-\beta^2). \tag{23}$$

To obtain an explicit form of $\mathcal{D}_1^h$ we integrate (23) and get

$$\mathcal{D}_1^h = \frac{(x^2+2)^{3/2}}{x} + \frac{(1-\beta^2)\sqrt{\beta^2+2}}{\beta}\ln\left[1+\beta^2+\frac{\beta^2(\beta^2+2)}{(L-x)^2}+\frac{\beta A}{(L-x)^2}\right] + A + \beta^2\ln[1+\beta^2+(L-x)^2+A],$$
$$A = \sqrt{(L-x)^2+\beta^2}\sqrt{(L-x)^2+\beta^2+2}. \tag{24}$$

Distributions of $\mathcal{D}_1^h$ and $\partial\mathcal{D}_1^h/\partial x$ are shown in Fig. 13. One can see that (1) with $c_a < 2$ ($\beta < 1$) the functional $\mathcal{D}_1^h$ is convex within the interval $(0, L)$, (2) with $c_a \to 2$ the coordinate of the minimum of $\mathcal{D}_1^h$ tends to L, in other words the mesh may be strongly condensed, (3) $\mathcal{D}_1^h$ has an infinite barrier preventing the right cell from collapsing. Analogous properties are exhibited in the 1-D case for any c_a (see [19]). With $c_a > 2$, when point 2 approaches point 3 and, consequently, $L - x \to 0$, the second term in (24) is dominant and has negative sign, since $1 - \beta^2 < 0$. In Fig. 13, one can see that $\mathcal{D}_1^h$ loses convexity when $c_a > 2$. It seems to lead the right cell to collapse when minimizing $\mathcal{D}_1^h$. However, up to a certain c_a it does not happen for the following reason. In the model example, the iterative procedure (16) is a Newton method and the coordinate of point 2 at the $l+1$th step is determined by the formula

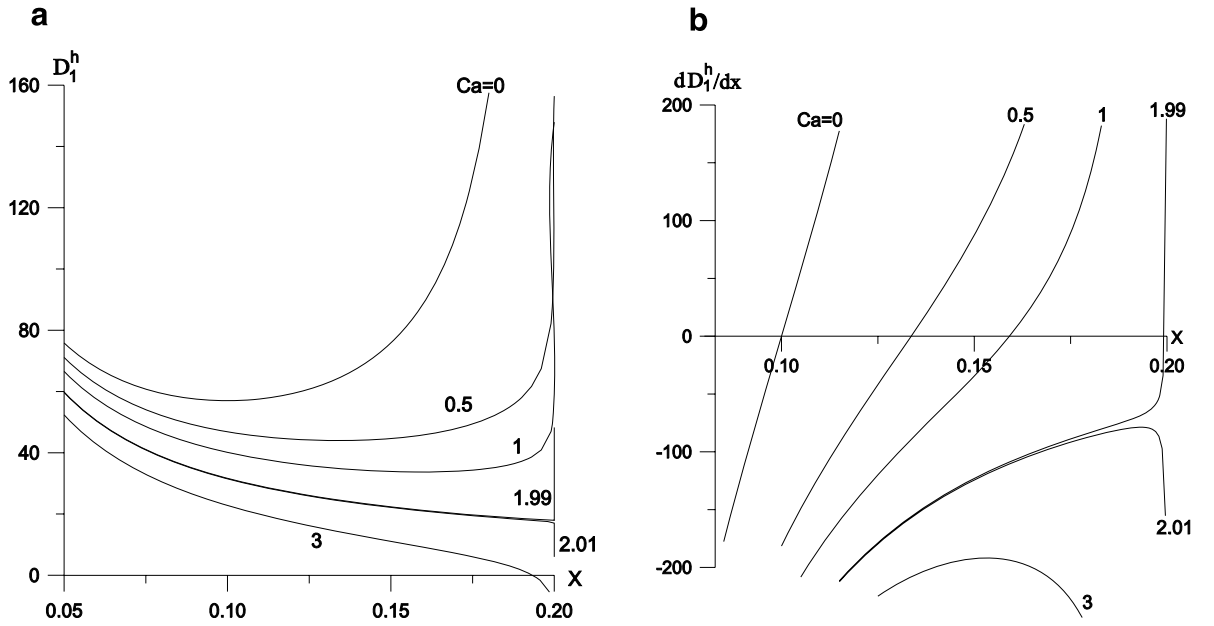

Fig. 13. Distributions of $\mathcal{D}_1^h$ (a) and $\partial\mathcal{D}_1^h/\partial x$ (b). With $c_a < 2$ there is infinite barrier and it disappears with $c_a \geqslant 2$.

$$x^{l+1} = x^l - \tau \frac{\partial \mathcal{D}_1^h}{\partial x}\left(\frac{\partial^2 \mathcal{D}_1^h}{\partial x^2}\right)^{-1}. \tag{25}$$

The second derivative of $\mathcal{D}_1^h$ is given by

$$\frac{\partial^2 \mathcal{D}_1^h}{\partial x^2} = \frac{2}{\sqrt{x^2+2}}\left(x + \frac{1}{x} + \frac{4}{x^3}\right) + \frac{(L-x)[((L-x)^2+\beta^2)^2 + (L-x)^2 + \beta^2] + 4}{0.5(L-x)^2\sqrt{(L-x)^2+\beta^2}\sqrt{(L-x)^2+\beta^2+2}}.$$

When $L - x^l \to 0$, retaining the terms of $O((L-x^l)^{-1})$ and $O((L-x^l)^{-2})$ in the first and second derivatives, respectively, one obtains in (25)

$$x^{l+1} - x^l = -\tau \frac{(\beta^2+2)(1-\beta^2)}{\beta^2+4}(L - x^l).$$

Since $\tau < 1$ and $1 - \beta^2 < 0$, it is obvious that the increment $x^{l+1} - x^l$ will be smaller than the distance to point 3 until the equality

$$-(\beta^2+2)(1-\beta^2)/(\beta^2+4) = 1$$

is fulfilled. From this we obtain $\beta \simeq 1.565$ or, for our example, $c_a \simeq 3.13$. Thus, the length of the right cell remains greater than zero within the interval $1 \leqslant \beta < 1.565$ ($2 \leqslant c_a < 3.13$). With $\beta > 1.565$ the right cell collapses. This is a distinction of the 2-D case where the iterations (25) hold $x^l < L$ for $c_a > 0$ (see [19]).

Thus, there are three intervals of $c_a = 2\beta/|u_r - u_l|$ for a discontinuous monitor function. In the first $0 < \beta < 1$, the functional $\mathcal{D}_1^h$ has an infinite barrier keeping the mesh from folding. In the second $1 \leqslant \beta < 1.565$, it reveals the barrier property of the iterative procedure preserving the right cell from collapsing. In the third interval $\beta > 1.565$, the adjacent nodes, located on both sides of the discontinuity surface, coincide and the mesh folds. It is worth noting that the second interval is unusable for practical computations. This model can be readily extended for any even number of cells $N_1 - 1 > 4$ in x.

The model considered explains the node motion mechanism in 3-D problems of hydrodynamics with a discontinuous monitor function f. In the neighborhood of a point of the discontinuity surface we may consider a local Cartesian system of coordinates with the x-axis directed along the normal to this surface. Then, to a first

approximation, one may assume $x = x(\xi)$, $y = a\eta$, $z = b\zeta$ and neglect the small terms with f_y, f_z. Behavior of the adaptive mesh near the discontinuity surface depending on c_a will be analogous to that of this model example.

To avoid mesh folding, we introduce one more parameter which determines the minimal thickness of the layer of high gradients of $\tilde{f} = c_a f$ and restricts a maximum gradient of $\tilde{f}$ [18]. First on the constructed mesh, we calculate the discrete nodal derivatives $\tilde{f}^h_x, \tilde{f}^h_y, \tilde{f}^h_z$ and specify a maximal value for the modulus of the gradient in the monitor function $F_{\max} = \chi \max(|\nabla \tilde{f}|)$, where $\chi < 1$ is a coefficient selected during computations. When adapting, we update the gradient of $\tilde{f}$ as follows

$$\nabla \tilde{f}^* = \begin{cases} F_{\max} \nabla \tilde{f} / |\nabla \tilde{f}| & \text{if } |\nabla \tilde{f}| > F_{\max}, \\ \nabla \tilde{f} & \text{if } |\nabla \tilde{f}| \leqslant F_{\max}. \end{cases}$$

Obtained values $\tilde{f}^*_x, \tilde{f}^*_y, \tilde{f}^*_z$ are substituted in (14) instead of $\tilde{f}^h_x, \tilde{f}^h_y, \tilde{f}^h_z$.

12. Conclusion

We have presented a variational method of constructing adaptive hexahedral grids. It is based on minimizing a functional. Adaptation is employed by mesh construction in the Riemannian manifold in $\mathbb{R}^{3+m}$ and subsequent projection down to the physical domain in $\mathbb{R}^3$. Grid construction is employed by the homeomorphic piecewise smooth mapping, being the union of the homeomorphic smooth mappings of every cell in the parametric domain onto the corresponding cell in the physical domain. The infinite barrier on the boundary of the set of non-folded grids, composed of dodecahedral cells, prevents grid degeneration during mesh construction. Corresponding hexahedral grids are also non-folded. A special case of a discontinuous monitor function was discussed. The use of the control metric allows employment of an additional control for the coordinate surfaces when adapting the mesh. The method can be employed in real engineering problems with complicated geometry of the physical domain. It may be extended to adaptive unstructured meshes in a straightforward manner.

Acknowledgments

The author is grateful to Prof. Olga Ushakova, Institute of Mathematics and Mechanics of Russian Academy of Sciences, Ekatherinburg, and Dr. Matthew Hubbard, University of Leeds, for helpful comments on this work. This work was supported by the Department of Mathematical Sciences of the Russian Academy of Sciences (Program 3).

References

[1] J.F. Thompson, Z.U.A. Warsi, C.W. Mastin, Numerical Grid Generation: Foundations and Applications, North-Holland, 1985.
[2] M.J. Baines, Moving Finite Elements, Clarendon Press, Oxford, 1994.
[3] S.A. Ivanenko, Adaptive-Harmonic Grid Generation, Computing Center of Russian Academy of Sciences, Moscow, 1997.
[4] J.F. Thompson, B.K. Soni, N.P. Weatherill (Eds.), Handbook of Grid Generation, CRC Press, Boca Raton, FL, 1999.
[5] V.D. Liseikin, Grid Generation Methods, Springer, New York, 1999.
[6] V.D. Liseikin, A Computational Differential Geometry Approach to Grid Generation, Springer, Berlin, 2006.
[7] J.F. Thompson, A survey of dynamically adaptive grids in the numerical solution of partial differential equations, Appl. Numer. Math. 1 (1985) 3–27.
[8] P.R. Eiseman, Adaptive grid generation, Comput. Meth. Appl. Mech. Eng. 64 (1987) 321–376.
[9] V.D. Liseikin, Construction of structured adaptive grids – a review, Comput. Math. Math. Phys. 36 (1) (1996) 1–32.
[10] S.A. Ivanenko, G.P. Prokopov, Methods of adaptive harmonic grid generation, Comput. Math. Math. Phys. 37 (8) (1997) 627–645.
[11] T. Tang, Moving mesh methods for computational fluid dynamics, Contemp. Math. 383 (2005) 141–173.
[12] J.U. Brackbill, J.S. Saltzman, Adaptive zoning for singular problems in two dimensions, J. Comput. Phys. 46 (1982) 342–368.
[13] D.A. Anderson, Equidistribution schemes, Poisson generators and adaptive grids, Appl. Math. Comput. 24 (3) (1987) 211–227.
[14] A.S. Dvinsky, Adaptive grid generation from harmonic maps on Riemannian manifolds, J. Comput. Phys. 95 (1991) 450–476.
[15] V.D. Liseikin, On generation of regular grids on *n*-dimensional surfaces, USSR Comput. Math. Math. Phys. 31 (11) (1991) 47–57.
[16] R. Hagmeijer, Grid adaptation based on modified anisotropic diffusion equations formulated in the parametric domain, J. Comput. Phys. 115 (1994) 169–183.

[17] A.A. Charakhch'yan, S.A. Ivanenko, A variational form of the Winslow grid generator, J. Comput. Phys. 136 (1997) 385–398.
[18] B.N. Azarenok, S.A. Ivanenko, Application of adaptive grids in numerical analysis of time-dependent problems in gas dynamics, Comput. Math. Math. Phys. 40 (9) (2000) 1330–1349.
[19] B.N. Azarenok, Variational barrier method of adaptive grid generation in hyperbolic problems of gas dynamics, SIAM J. Numer. Anal. 40 (2) (2002) 651–682.
[20] B.N. Azarenok, S.A. Ivanenko, T. Tang, Adaptive mesh redistribution method based on Godunov's scheme, Comm. Math. Sci. 1 (1) (2003) 152–179.
[21] H.Z. Tang, T. Tang, Adaptive mesh methods for one- and two-dimensional hyperbolic conservation laws, SIAM J. Numer. Anal. 41 (2003) 487–515.
[22] B.N. Azarenok, T. Tang, Second-order Godunov-type scheme for reactive flow calculations on moving meshes, J. Comput. Phys. 206 (2005) 48–80.
[23] S.A. Ivanenko, Harmonic mappings, in: J.F. Thompson, B.K. Soni, N.P. Weatherill (Eds.), Handbook of Grid Generation, CRC Press, Boca Raton, FL, 1999 (Chapter 8).
[24] G. Liao, F. Liu, G.D. Pena, D. Peng, S. Osher, Level-set-based deformation method for adaptive grids, J. Comput. Phys. 159 (2000) 103–122.
[25] S.A. Ivanenko, A.A. Charakhch'yan, Curvilinear grids of convex quadrilaterals, USSR Comput. Math. Math. Phys. 28 (2) (1988) 126–133.
[26] S.K. Godunov, G.P. Prokopov, On computation of conformal transformations and construction of difference meshes, USSR Comput. Math. Math. Phys. 7 (1967) 209.
[27] S.A. Ivanenko, Control of cell shape in the construction of a grid, Comput. Math. Math. Phys. 40 (11) (2000) 1596–1616.
[28] B.N. Azarenok, A variational hexahedral grid generator with control metric, J. Comput. Phys. 218 (2006) 720–747.
[29] S.A. Ivanenko, Variational methods for adaptive mesh generation, Comput. Math. Math. Phys. 43 (6) (2003) 793–806.
[30] S.K. Godunov, V.T. Zhukov, O.V. Feodoritova, On one class of quasi-isometric grids, in: O.V. Ushakova (Ed.), Advances in Grid Generation, Nova Science Publishers, New York, 2007 (Chapter 2).
[31] S.A. Ivanenko, B.N. Azarenok, Grid optimization and adaptation, in: O.V. Ushakova (Ed.), Advances in Grid Generation, Nova Science Publishers, New York, 2007 (Chapter 4).
[32] G.P. Prokopov, Moving mesh calculation in unsteady two-dimensional problems, in: O.V. Ushakova (Ed.), Advances in Grid Generation, Nova Science Publishers, New York, 2007 (Chapter 5).
[33] O.V. Ushakova, Nondegeneracy conditions for different types of grids, in: O.V. Ushakova (Ed.), Advances in Grid Generation, Nova Science Publishers, New York, 2007 (Chapter 9).
[34] O.V. Ushakova, Conditions of nondegeneracy of three-dimensional cells. A formula of a volume of cells, SIAM J. Sci. Comp. 23 (4) (2001) 1273–1289.
[35] B.N. Azarenok, A scheme for detonation wave computation on moving meshes, Comput. Math. Math. Phys. 45 (12) (2005) 2174–2195.
[36] R. Schoen, S.T. Yau, On univalent harmonic maps between surfaces, Invent. Math. 44 (1978) 265–278.
[37] N.A. Bobylev, S.A. Ivanenko, A.V. Kazunin, Piecewise smooth homeomorpisms of bounded domains and their applications to the theory of grids, Comput. Math. Math. Phys. 43 (6) (2003) 772–781.
[38] S.S. Sritharan, Mathematical aspects of harmonic grid generation, in: J.E. Castillo (Ed.), Mathematical Aspects of Numerical Grid Generation, SIAM, Philadelphia, 1991 (Chapter 10).
[39] C.W. Mastin, J.F. Thompson, Transformation of three-dimensional regions onto rectangular regions by elliptic systems, Numer. Math. 29 (1978) 397–407.
[40] A. Winslow, Numerical solution of the quasi-linear Poisson equation in a nonuniform triangle mesh, J. Comput. Phys. 1 (1967) 149–172.
[41] H. Liu, G. Liao, A note on harmonic maps, Appl. Math. Lett. 9 (4) (1996) 95–97.
[42] R.S. Laugesen, Injectivity can fail for higher-dimensional harmonic extensions, Complex Variables 28 (1996) 357–369.
[43] P. Knupp, R. Luczak, Truncation error in grid generation: a case study, Numer. Meth. Partial Diff. Eq. 11 (1995) 561–571.